Integrated dynamic testing and analysis approach for model validation of an innovative wind turbine blade design

Luczak, Marcin; Peeters, B.; Manzato, S.; di Lorenzo, E. ; Csurcsia, P. Z.; Reck-Nielsen, Kasper; Berring, Peter; Haselbach, Philipp Ulrich; Branner, Kim; Ruffini, Valentina

Publication date:
2018

Document Version
Publisher's PDF, also known as Version of record

Integrated dynamic testing and analysis approach for model validation of an innovative wind turbine blade design

M.M. Luczak[1], B. Peeters[2], S. Manzato[2], E. Di Lorenzo[2], P. Z. Csurcsia[2,5], K. Reck-Nielsen[3], P. Berring[1], P. U. Haselbach[1], K. Branner[1],V. Ruffini[4]
[1] Technical University of Denmark, Department of Wind Energy
Frederiksborgvej 399, 4000, Roskilde, Denmark
e-mail: **mluz@dtu.dk**

[2] Siemens Industry Software NV, RTD Test Division
Interleuvenlaan 68, 3001, Leuven, Belgium

[3] CEKO Sensors ApS
Diplomvej 381, DK-2800 Kgs. Lyngby, Denmark

[4] University of Bristol, Faculty of Engineering
Queen's Building, University Walk, Clifton BS8 1TR, UK

[5] Vrije Univeriteit Brussel, Department of Engineering Technology
Pleinlaan 2, 1050 Elsene, Belgium

Abstract
DTU Wind Energy continues the experimental investigation of the wind turbine blades to assess innovative designs of long and slender blades. This paper presents an experimental structural dynamics identification and structural model validation of the 14.3m long research blade. Unique feature of the blades is that its internal layup design has been highly optimized w.r.t. stretching the rotor and substantial mass reduction at the same time. As the result, the blade is more flexible than the traditional one. The results of the modal tests following analyses were performed: (i) Uncertainty Quantification of the experimental modal parameters for the blades, (ii) non-linearity assessment, (iii) numerical model correlation – frequencies and mode shapes of the experimental model comparison with those from Finite Element (FE). Finally, the outlook for the future experimental blade research activity is outlined.

1 Introduction

Modern wind turbine blades are expected to withstand the in-service and extreme loads for a lifetime of 25 years. The IEC 61400-23 standard [1] requires full-scale structural testing of wind turbine blades. The standard defines the static load, fatigue load and natural frequencies testing and interpretation of the results. Requirements for the structural dynamic identification are limited to measurements of the first and second flapwise and first edgewise frequencies. Remaining blade modal properties such as damping and mode shapes are listed under the optional tests.

The length of recently developed offshore wind turbine blades exceeds 100 meter [2]. In-depth understanding of the dynamic behavior of such slender and flexible structures requires detailed experimental investigation exceeding the current scope required by the standard since unstable vibrations of wind turbine

blade may lead to its failure. Adequate identification of the blade‘s mode shapes is critical for the analysis of stability problems. Experimental modal testing is a well-established tool [3-5] for the estimation of the modal model of a mechanical system. At DTU Wind Energy (former Risø National Laboratory), modal testing has been applied to full-scale wind turbine blades. The work of Larsen et al [6] and Pedersen et al [7] revealed some discrepancies between experimentally and numerically obtained mode shapes. Large differences were observed especially for torsional modes. Extensive and well documented activities on modal testing of research-scale blades was conducted at Sandia National Laboratory. Different support configurations for the investigated blades have been studied [8] followed by the uncertainty analysis of the obtained results [9]. Uncertainty quantification has been a subject of investigations for the modal test of helicopter rotor blades [10]. The test setup has been found to have a large effect on the performed tests, as the mass of the sensors or damping added from cables may significantly influence the values of the observed frequencies and damping. Furthermore, the influence of the support structure has also been taken into account in the parameter estimation and numerical model validation [11].

Progress in the development of measurement equipment has enabled application of different sensors for modal testing of wind turbine blades. Optical methods are commonly used for full-field blade response measurement [12-14]. One of the main advantages of the application of camera-based full field methods is the collection of strain and acceleration data combined in one measurement system. Strain modal analysis [15] is an attractive alternative for vibration acceleration measurements, as the blade is often instrumented with a dense network of strain gauges for static and fatigue testing. Alternative excitation methods are being investigated with the application of Piezoelectric Transducer (PZT) patches as actuators [16].

Characterization of blade dynamics is one area of the modal testing results application. The modal models are also used for the numerical model validation for the model improvement [17, 18] and damage detection [19].

This paper presents a study on the integrated dynamic testing and analysis for model validation of a research-scale wind turbine blade. Section 2 describes the experimental setup and measurement results. Section 3 provides information on the validation of the FE model of the blade. The final section concludes on the research done so far and sets the future outlook.

2 Numerical modal analysis

The blade was modelled using the commercial finite element package pre/post-processing software MSC Patran (version 2014). The model was generated by using Risø-DTU’s in-house software Blade Modeling Tool (BMT). MSC Marc was applied as the solver in all analyses.

The blade structure was discretized using 20-noded layered continuum solid elements, which requires a volume representation of the geometry. The entire blade geometry was modelled based on input data of 99 blade cross sections generated by DTU Wind Energy’s in-house Beam Cross section Analysis Software (BECAS) optimizing scheme [20]. The blade airfoil defines the outer cross-section geometry. An offset according to the layup and layer thickness of the composite material determines the element thickness. Finally, the individual cross-sections were connected by spline curves and interpolation surfaces to obtain a volume representation of the blade. This process was handled automatically by BMT, which uses 60 regions/solids to assign the different cross-sectional properties computed by the BECAS optimizing scheme. Figure 1 shows segments of the blade model.

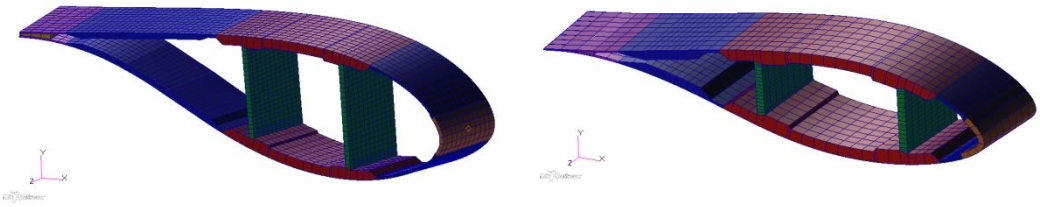

Figure 1: Left: Cross-section segment at radial position of around 5m, right: mid segment.

Depending on the region, the composite layup consists of 6 to 32 plies through the thickness. The properties of the composite, with its material, layup and ply orientations were assigned to 20-noded layered continuum elements defining the element stiffness matrix. The model was discretized with approximately 130,000 layered 20-noded continuum elements.

The blade manufacturer has not stated the exact properties for the fibers and matrix material, so properties from comparable materials described in the literature have been used to some extent. For this purpose, the elastic properties were calculated using Autodesk Simulation Composite tool, which uses a calculation scheme based on the Classical Laminate Theory. The estimated characteristic mechanical material properties and the estimated design material strengths applied in these studies are presented in Table 1.

Mechanical properties	**UNIAX**	**BIAX**	**TRIAX**	**Chop**	**Core**	**Glue**	**Gelcoat**
E1 [MPa]	37800	9550	18700	13600	48.5	3009	2000
E2 [MPa]	11100	9550	10900	13600			
G12 [MPa]	3270	10100	7720	5130			
ν_{12}	0.24	0.62	0.55	0.32	0.4	0.3	0.3
ϱ [kg/m^3]	1850	1780	1780	1684	80	1540	1500
Thickness [mm]	0.95	0.5	0.75	0.3	5-10	-	0.6
Design strength (PSF 2.205)							
X_T [MPa]	360.0	69.3	186.0	56.2	x	x	x
X_C [MPa]	257.0	64.9	152.0	56.2	x	x	x
Y_T [MPa]	24.8	69.3	30.5	56.2	x	x	x
Y_C [MPa]	63.5	64.9	51.5	56.2	x	x	x
S [MPa]	16.6	55.9	42.3	23.9	x	x	x

Table 1: Material properties

The natural frequencies and mode shapes of the blade are shown in Table 2:

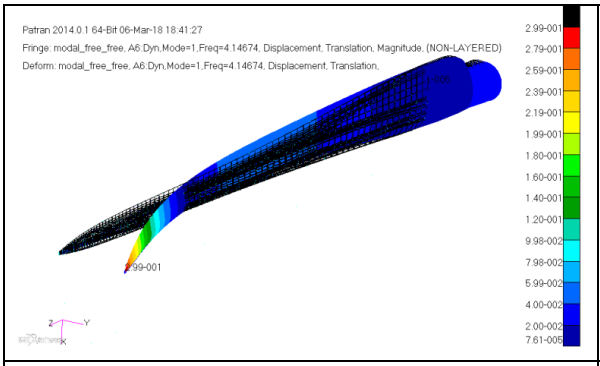	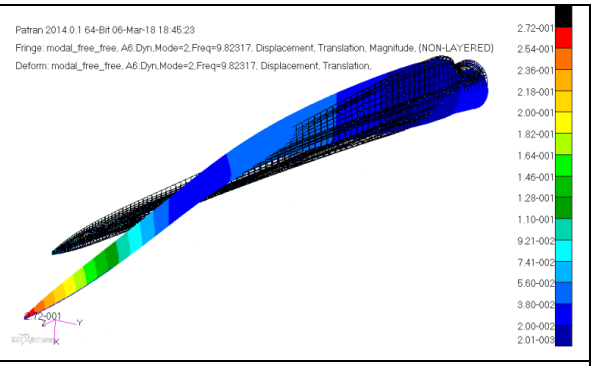
1st Flapwise FE mode 4.12 [Hz]	1st edgewise FE mode 9.87 [Hz]
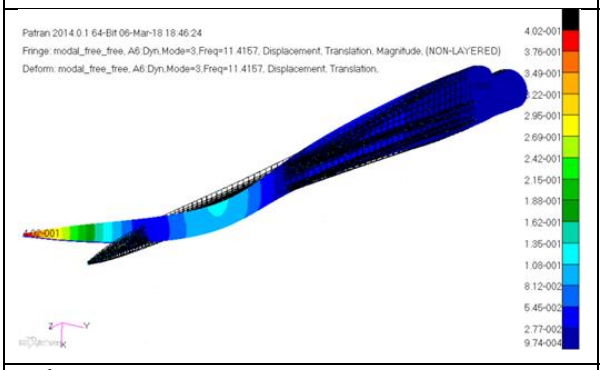	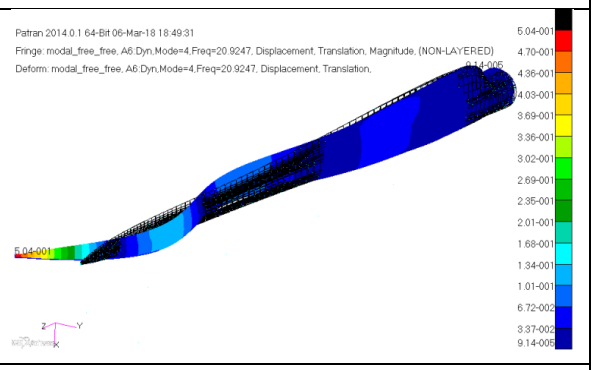
2nd Flapwise FE mode 11.36 [Hz]	3rd Flapwise FE mode 20.81 [Hz]

Table 2 Mode shapes examples from FEM analysis

3 Experimental modal analysis

DTU Wind Energy department has recently commissioned a Large Scale Test Facility built for the experimental research of full-scale wind turbine blades and their subcomponents. The facility has three test rigs capable of accommodating blades of different lengths, ranging from 12 up to 45 meters, for static, fatigue and dynamic testing as shown in Figure 2.

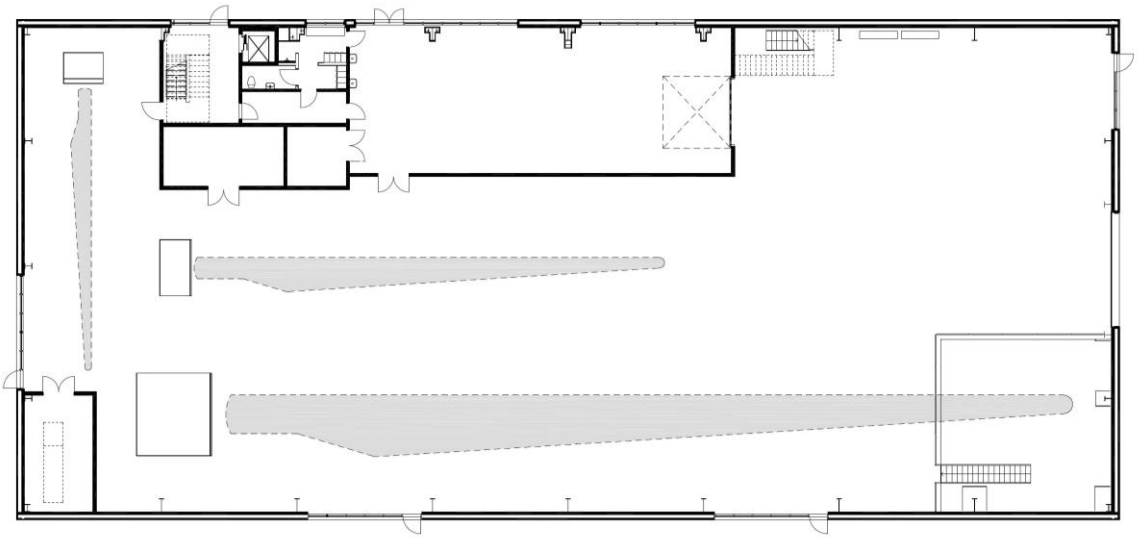

Figure 2 Large Scale Test Facility layout with three test rigs for a full scale blade tests.

The blade tested for this study is a research-scale blade, with a length of 14.3 m and a mass of approximately 530 kg. It has been entirely designed at the DTU Wind Energy department, and manufactured by Olsen Wings. Modal tests have been performed before destructive static and fatigue testing. An estimated modal model of the intact blade will serve as a reference data for the post-fatigue damage detection. After the fatigue testing, the modal tests will be repeated and the results will be compared to the initial modal analysis data. In addition, blade modal models will be analyzed in order to investigate the detection possibilities of damage in the blade.

3.1 Test setup

In the presented measurement campaign, the test blade was supported with two elastic cords in the edgewise direction to provide free-free boundary conditions as presented in Figure 3. This configuration is particularly convenient for the updating of the numerical model of the blade, as it does not require modelling of the boundary conditions.

The investigated blade has been simultaneously excited in the flapwise and edgewise directions with two electrodynamic shakers. As measurement grid, it was decided to split the blade into 15 equidistant “stations”, one every 1m. Additionally, each station was measured at 8 locations (Figure 4) , including: the trailing and leading edge, the point of maximum stiffness on the pressure and suction sides of the airfoil, plus 4 intermediate points between these. The high-fidelity finite element model presented in the previous section was used to simulate the test results and optimize sensor placement, in terms both of coordinates and orientation. Using the proposed locations, it was verified that the current measurement setup could guarantee a good description of the first 30 modes.

To ensure a consistent and repeatable excitation of the blade, and avoid damaging it, two relatively stiff points on the flap and edgewise directions were selected. As shown in Figure 3, the shaker along the edgewise direction was placed approximately in the middle of the blade, close to the expected nodal line of the first edgewise mode, to keep the maximum resonant response of the blade to safe levels. For the horizontal shaker, a point close to the center of gravity was selected. However, ensuring a good connection of the shaker to the blade in this direction has been more difficult, as in this direction the blade responds like a pendulum, causing the stinger to detach often from the blade. In addition, as the stingers were disconnected from the blade after each run before moving the accelerometers, a consistency check was performed to ensure the system remained invariant over the different test runs.

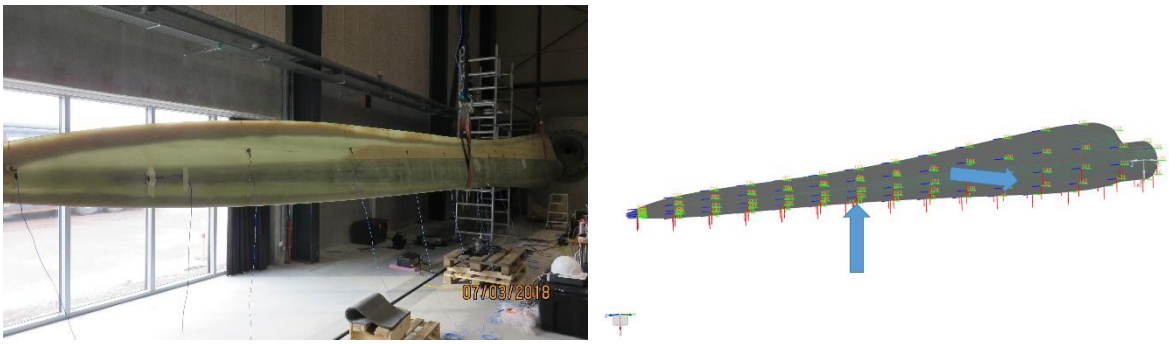

Figure 3 Instrumented blade on the test stand in the free-free support configuration (left) and geometry of the measurement and excitation points (right).

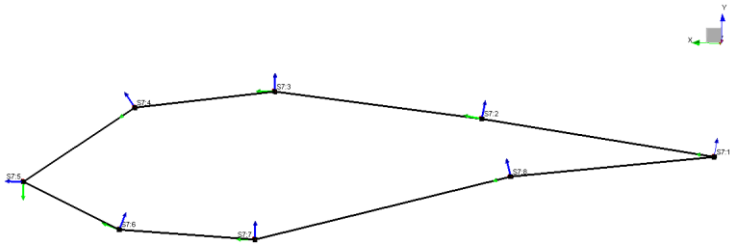

Figure 4: Sensor instrumentation along the airfoil.

The excitation forces and the corresponding driving-point Frequency Response Functions (FRFs) were measured by two impedance heads, which encapsulate force and acceleration sensors in one housing. The dynamic response of the blade was measured with 15 tri-axial piezoelectric accelerometers. Considering the total number of degrees-of-freedom on the measured grid (15 stations x 8 locations x 3 directions = 360 DOFs) it was decided to perform the measurement in a roving accelerometer configurations, so that the 15 sensors were moved over the 8 locations for each measurement station. As the driving-point FRFs at the excitation locations were measured for all runs, they are used as reference to recombine the different datasets and scale the mode shapes.

3.2 Uncertainty analysis

In this section, the main sources of uncertainties that were analyzed correspond to the measurement setup. As discussed in the previous section, the whole measurement grid was covered in 8 runs, where the excitation was applied always at the same location while the accelerometers were moved around the profile of the airfoil. Moreover, as the two stingers connecting the shakers to the blade were disconnected before moving the accelerometers, inconsistencies in the actual direction of application of the force could arise. Variations in modal parameters between the different runs can therefore be attributed to:

- Misalignment of the stinger axis,
- Loose connection between shakers and structure,
- Time of measurements (campaign was performed over a period of 3 days, with significantly different meteorological and temperature conditions),
- Mass loading effects due to accelerometers and cables (this is considered to be negligible considered the total mass of the blade),
- Change in the stiffness of the supporting elastic cords over time.

In Figure 5 the variability of the excitation over the 8 runs is shown. For the excitation in the edgewise direction, the Driving Point FRFs are highly repeatable and consistent. On the other hand, the corresponding flapwise Driving Points show much higher variability between the different runs, because of the difficulties in ensuring a good and reliable connection between the shaker and the blade.

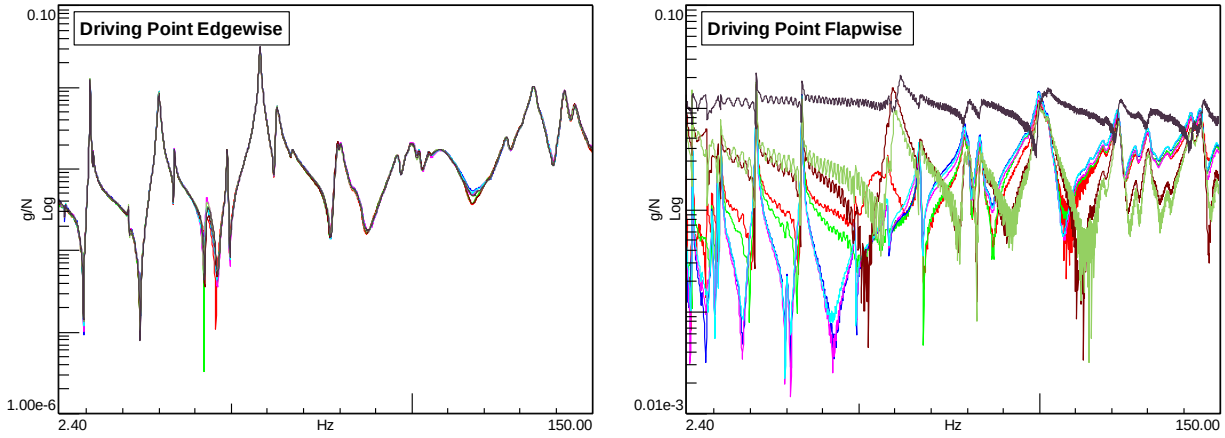

Figure 5: Driving Point FRF for the edgewise and flapwise excitation over the 8 different runs

Starting from these observations, modal analysis was performed on the 8 datasets and the individual estimates are compared. The following procedure was applied:

1. The Polymax modal parameter estimation was applied to the FRFs collected during each run using the same settings: (i) a maximum model order of 100 was set to estimate modes in the 2.5 to 150 Hz frequency band; (ii) upper and lower residuals were included; (iii) poles were selected manually; and (iv) modes were assumed to be complex.
2. Only modes consistently appearing in all modesets were included in the statistical calculation.
3. For each mode, the average and the standard deviation of the frequency and damping were computed.
4. Individual estimates were normalized to the corresponding average value to simplify visualization.
5. To correlate the results with the actual test, the average coherence on the edgewise driving point is also added to the plot.

The results of the analysis are displayed in Figure 6 both for the frequencies and damping. In general, the scatter of the estimates is very limited between the different runs. For the frequencies, we observed some higher variability in correspondence of the first mode (the 1st flapwise bending), the torsional mode around 43 Hz, and finally on a cluster of modes between 100 and 110 Hz. For the damping, a larger variability can also be observed at higher frequency, around 130 Hz. A higher uncertainty on the damping can generally be expected as damping estimates are more sensitive to inconsistencies in the data and on the selection of one specific pole in the stabilization diagram. In general, however, despite the difficulties in connecting the flapwise shaker to the structure, the actual duration of the test over few days and the roving of the accelerometers, the results are quite consistent and as a consequence, the FRFs from the different runs can be processed all together into a single database.

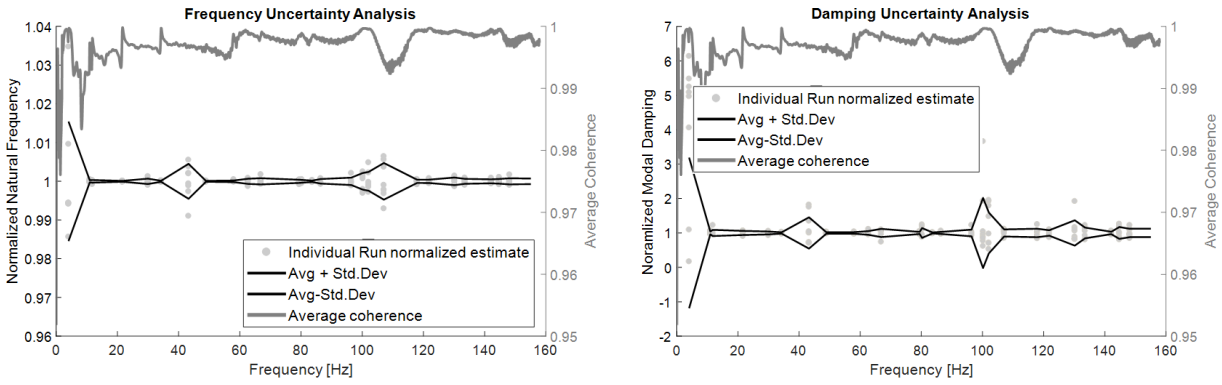

Figure 6: Modal Frequency and Damping uncertainty analysis results.

3.3 Nonlinearity assessment

In modern system identification special excitation signals are available to assess the underlying systems in a user-friendly, time efficient way [21]. In order to avoid any spectrum leakage, to reach full nonparametric characterization of the noise, and to be able to detect nonlinearities, a periodic signal is needed. Many users prefer noise excitations, because they are simple to implement, but in this case nonlinearities are not identifiable, and there is a possible leakage error.

3.3.1 Multisine excitation technique

The best signal that satisfies the properties listed above is the multi-sine signal (see Figure 7), which looks and behaves like Gaussian white noise, but is deterministic. It is important to highlight that multi-sine excitation is not equivalent to stepped sine excitation [22,23].

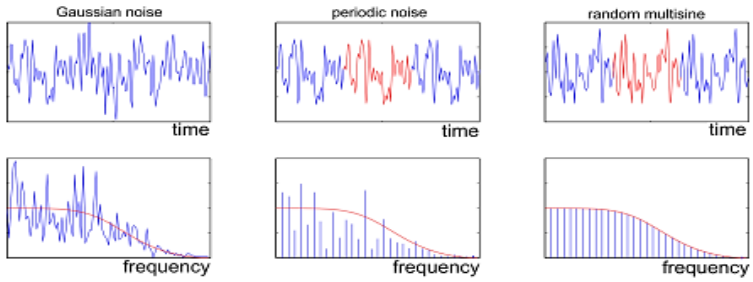

Figure 7 Different excitation signals in time and in frequency domain

3.3.2 Best Linear Approximation approach

The Best Linear Approximation (BLA) method has been widely used in the last decades to efficiently estimate FRFs [21, 24, 25]. The BLA of a nonlinear system minimizes the mean square error between the true output of a nonlinear system and the output of the linear model, see Figure 8. With this technique, instead of using the classical H1 estimate (cross-power spectral density estimate [21]) and its coherence function, a BLA model is estimated, and the coherence function is split into a) noise level and b) nonlinear contribution estimates.

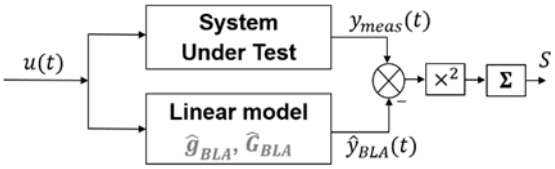

Figure 8 The baseline model and the cost function (S) of the best linear approximation framework

The proposed BLA technique makes use of the knowledge that the excitation signal has both stochastic and deterministic properties. In this work, random phase multi-sines are used and generated in the frequency domain such that the magnitude is set by the user, and the phases of the cosines are chosen randomly from a uniform distribution [26].

A further difference w.r.t. H1 estimation is that instead of directly using the averaged input and output data, a partial BLA estimate is calculated for each period of the excitation, and several different realizations of the excitation signal are repeated multiple times. A BLA FRF estimate, for a given signal, is then calculated

via the average of different BLAs. In this case it is possible to easily estimate the noise levels and standard deviation of the estimates at each frequency line. The difference between the total variance of BLA and the noise variance is an estimate of the variance of the stochastic nonlinear contributions. In [22] it has been shown that the above statements are only true when some additional assumptions are satisfied.

3.3.3 Measurement analysis

Multiple multisine experiments have been done at relatively low and high power levels as it is recommended for the BLA measurement procedure [24].

Figure 9 shows the magnitude spectrum of the flapwise measured excitation signal at low (left figure, grey line) and high (right figure, black line) levels (with an approximate overall signal level difference of 10 dB, i.e. factor of 3). The reference signal – a computer-generated ideal waveform – has a completely flat magnitude. The differences between the ideal flat and measured magnitude characteristic, and the level of nonlinearities w.r.t the noise level illustrate the dynamic behaviour of the shaker and its interaction with the underlying structure. Black dots show the corresponding noise level estimates, which gives a rough estimate of the SNR (around 46 dB at low level excitation at mid frequencies, and around 50 dB at high level excitation). Orange and blue dots refer to the odd and even nonlinearities on the non-excited detection lines (the frequency bins where the type of nonlinearities can be captured). The even nonlinearities – compared to the noise level – become dominant at the high-level excitation profile, especially above 60 Hz. A further interesting thing to mention is that the influence of electrical noise (harmonics of the mains frequency 50 Hz) is less significant at the higher level excitation. Apart from this, the nonlinearities have limited effect, as they are of the same order as noise.

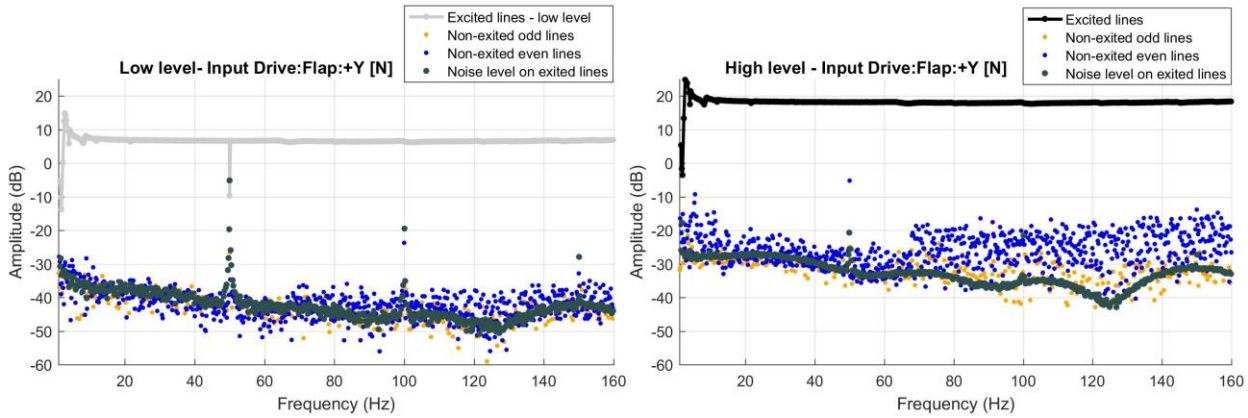

Figure 9 The measured excitation spectrum on the Y (flap) direction is shown for low level (gray line, on the left side) and high levels (black line, on the right side) together with the estimated noise level (black dots), even (blue dots) and odd (orange dots) nonlinearities.

Figure 10 shows the frequency response matrix estimate of the underlying system in the X and Y directions at the output channel S13, close to the wing tip. Black and grey lines show the high and low level FRFs with the corresponding noise (black and grey dots) and nonlinearity (red and orange dots) estimates. The low-level FRFs below -60 dB are quite noisy, and the nonlinearities have a limited effect (their level is approximately 5 dB higher than the noise). At the high excitation level, the SNR is significantly improved, but the level of the nonlinearities increases as well. From these results, it is also possible to see that the torsional mode at 42 Hz exhibits a particularly large difference in level between noise and nonlinearity, at both low and high excitation levels. In general, the nice overlay between the BLA and the measured FRFs is an indication that the system can be reasonably assumed to behave linearly. These results warrant further investigation of the behavior of this mode.

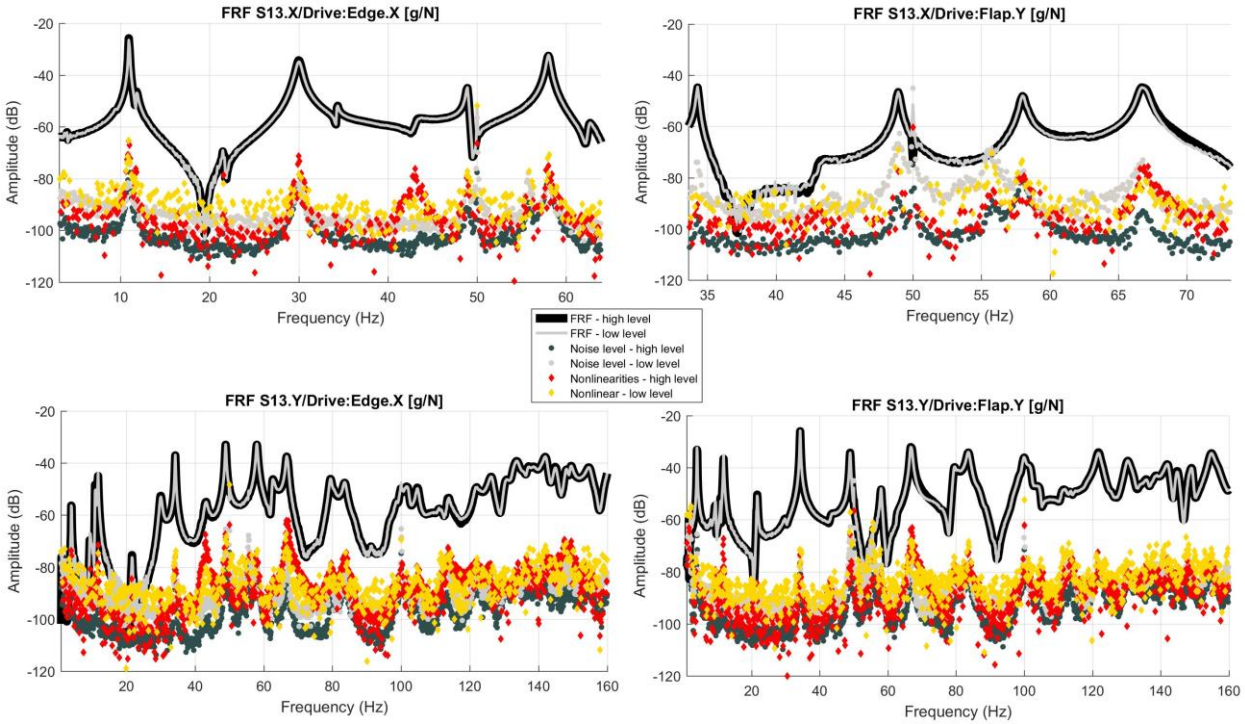

Figure 10 The best linear aproximation of the frequency response matrix is shown for low level (gray line) and high levels (black line) together with the estimated noise (grey and black dots) and nonlinearity (orange and red dots) levels at S13 channel.

3.4 Measurement results

Based on the preliminary observation and analysis performed in Sections 3.2 and 3.3, here a summary of the identified modes is given. Because of the repeatability between the different test runs, it was decided to fit a model including all FRFs at the same time, so that the fitted FRF and mode shapes can be more consistent to the actual blade behavior.

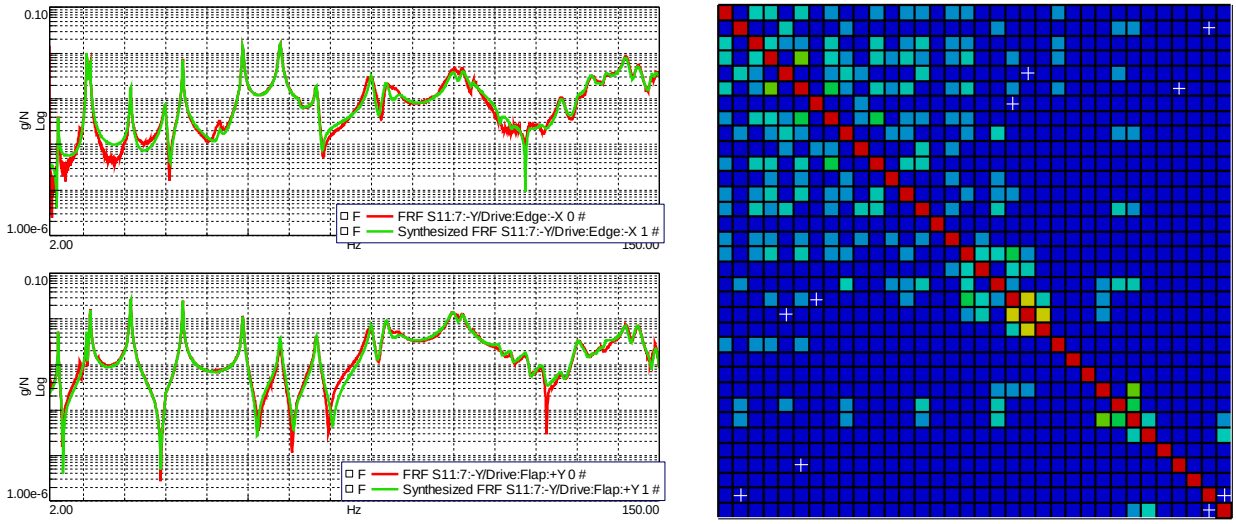

Figure 11: Validation of the identified modal model. Left: Comparison of measured (red) and synthesized (green) FRFs for a specific DOF (S11:7:-Y). Right: AutoMAC for the selected modeset.

In total, 33 modes have been reliably identified in the frequency range between 2 and 150 Hz. Figure 11 shows the validation of the modeset identified from the measured experimental data. On the left, the synthesized FRFs between one measured Degree of Freedom and the two excitations are displayed. In both cases, the correlation between the measured and reconstructed FRFs is very high, confirming that the identified model is able to correctly represent the structure in the frequency range of interest. On the right, the AutoMAC (autocorrelation between all mode shapes) is displayed: as the matrix has a dominant diagonal, the identified set contains independent vector and can thus be reliably used to validate (and later update) the numerical model from Section 2.

3.5 Optical accelerometer measurements

Mode	Frequency, Optical [Hz]	Frequency, Reference [Hz]	Deviation [%]
1	4.100	4.048	1.280
2	9.300	9.430	1.380
3	11.000	10.966	0.310
4	11.800	11.807	0.060
5	21.699	21.655	0.200
6	30.149	29.982	0.560
7	34.299	34.290	0.030

Figure 12 The optical accelerometer (CEKO OA1) was mounted flap-wise on the test blade. The accelerometer measures 27 mm in diameter. The first 7 resonance frequencies measured using the optical accelerometer and a reference piezoelectric accelerometer are shown in the table.

Two uniaxial all-optical MEMS accelerometers (CEKO Sensors, model OA1) were used to measure the transfer function of the test blade. The optical accelerometers are completely metal-free, thus immune to electromagnetic interference from e.g. lightning strikes, and therefore safe to operate on wind turbines under all conditions. They are based on refractive index modulation technology, which is a high sensitivity frequency modulated sensing principle. The accelerometers were mounted 12.5 m and 9 m from the root, respectively. Data was recorded using a CEKO Sensors S-DAS monitoring system operating at a 3000 Hz sampling rate. A piezoelectric accelerometer was located next to the optical accelerometer as reference. The measured transfer functions for the optical and piezoelectric accelerometer during pseudorandom excitation are seen in Figure 13. Figure 13 Comparison of measured transfer functions. Numerically calculated resonance frequencies are shown with dashed lines.Both the reference and the optical accelerometer detects practically all resonances below 100 Hz, though some have very low amplitudes due to the measurement locations. Differences in amplitudes are primarily due to the two accelerometers measuring along slightly different angles. At the 9 m position the amplitude of the fundamental mode is reduced compared to the resonances around 30 Hz. This is expected as this location is close to a node of the fundamental mode. The absolute error between resonance frequencies measured using the optical accelerometer and those of the piezoelectric reference, as well as the numerically calculated frequencies, is of the order of 1% or less.

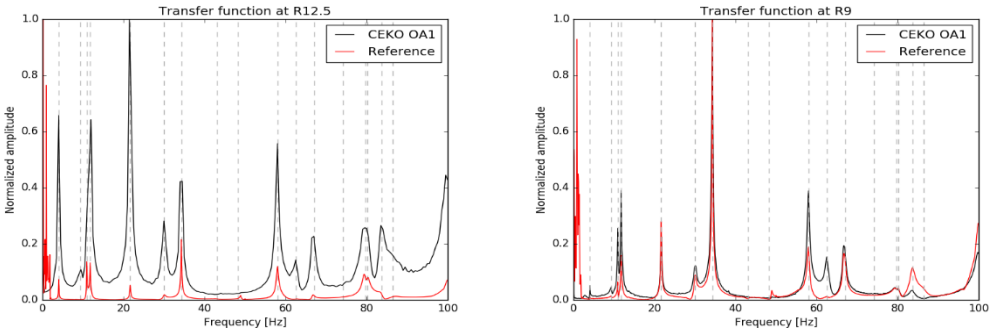

Figure 13 Comparison of measured transfer functions. Numerically calculated resonance frequencies are shown with dashed lines.

4 Test-simulation correlation

The numerical model described in Section 2 was validated with the experimental model identified in Section 3.4. As the experimental grid was derived from the numerical model, no geometric correlation is required as the measurement points already coincide with a node in the model. Consequently, the Modal Assurance Criterion between the numerical and experimental model can be calculated, and the results are displayed in Figure 14. Generally good correlation can be seen for the first 13 modes, while at higher frequencies the model and the experiments start to diverge. This is to be expected as the modal response at higher frequency is more localized and subject to uncertainties.

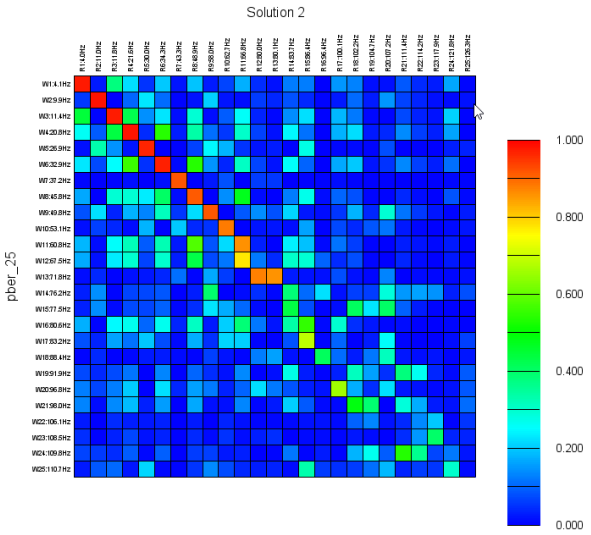

Figure 14 Modal Assurance Criterion between the numerical and experimental mode shapes

Test	FEM	MAC	Freq. % Error
4.05	4.13	0.98	2.14
10.96	9.87	0.98	-9.91
11.80	11.36	0.97	-3.71
21.65	20.81	0.98	-3.86
29.98	26.89	0.96	-10.31
34.28	32.86	0.97	-4.16
43.30	37.25	0.92	-13.98
48.93	45.76	0.91	-6.49
58.00	49.85	0.92	-14.06
62.67	53.14	0.88	-15.20
66.84	60.82	0.86	-9.00
80.00	71.75	0.87	-10.31
86.41	83.19	0.69	-3.73
100.10	96.78	0.66	-3.32
111.40	109.80	0.53	-1.44
133.59	110.73	0.59	-17.11

Table 3: Results of correlation analysis between test and simulation results

Based on the correlation between the modes, Table 3 compares the numerical and experimental natural frequency of matching modes. Here, only modes that show a correlation above 50% are compared and 16 pairs are reported. In general, very good agreement is found between all modes with a dominant flapwise direction, with errors between the natural frequencies ranging between 1 and 5%. Bigger discrepancies (with errors around 10%), on the other hand, are observed for the modes in the edgewise and torsional direction. Before drawing further conclusions, it is necessary to include the bungee cords used to suspend the blade in

the model, as they add stiffness in the edgewise direction. Indeed, the natural frequencies of the numerical model in this direction are consistently softer than the experimental results. In general, the good correlation between the global modes at low frequencies gives confidence in the general validity of the model, and an update of the material properties is not deemed necessary at this stage. In Figure 15, a comparison of some of the mode pairs is given.

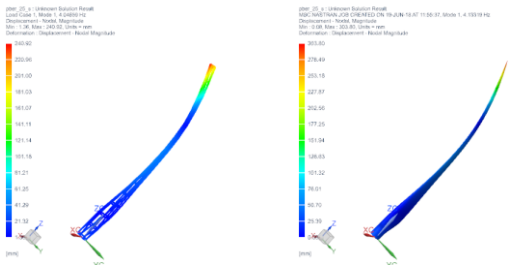

1st Flapwise Bending (4.05-4.12 Hz)

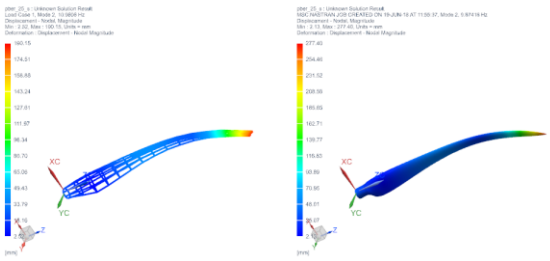

1st Edgewise Bending (10.96 – 9.87 Hz)

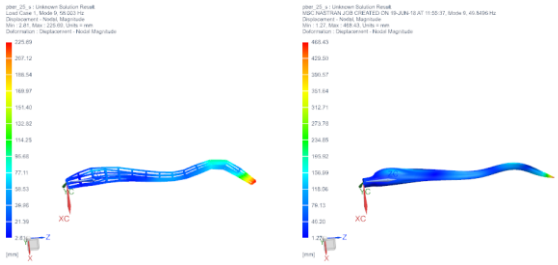

2 Edgewise Bending (58 – 49.85 Hz)

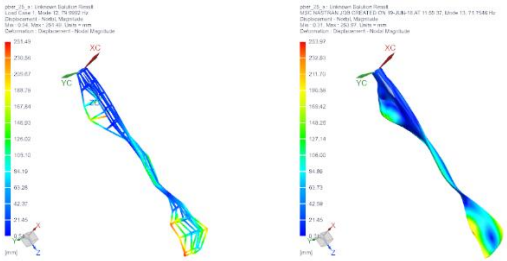

2nd Torsion (80 – 71.75 Hz)

Figure 15 Examples of experimental and numerical identified mode shapes.

5 Conclusions and future outlook

This paper presented dynamic testing and analysis for model validation of an innovative wind turbine blade design. Motivation for the work was to investigate the dynamic properties of the blade to a larger extent than required by a certification standard and apply the results for the blade model validation. An experimental modal analysis was implemented and provided an estimation of the full modal model parameters in the wide frequency band. Uncertainty quantification has confirmed high consistency in the experimental data collection. Based on this analysis result, the estimated experimental modal model was a credible reference for the validation of the numerical model. Performed tests did not show the presence of nonlinearity. Both uncertainty and nonlinearity analysis revealed problem with the precision of the identification of the torsional mode. Within the test campaign use of the innovative optical accelerometer has been successfully demonstrated. Future work will encompass use of the operational modal analysis for the blade bolted to the concrete block of the test rig. A certification standard requires static and fatigue testing with the use of the strain gauges. Therefore it is planned to use a test setup and the blade instrumentation for the vibration test.

Acknowledgements

The experimental work described herein has been conducted using mechanical testing and measurement equipment from Villum Center for Advanced Structural and Material Testing (CASMaT). The support from Villum Fonden (Award ref. 00007293) is gratefully acknowledged.

This work was supported by the Danish Centre for Composite Structures and Materials for Wind Turbines (DCCSM), Grant no. 09-067212 from the Danish Strategic Research Council.

The work is supported by the Danish Energy Agency through the Energy Technology Development and Demonstration Program (EUDP), Grant No. 64016-0023. The supported project is named ‘‘BLATIGUE: Fast and efficient fatigue test of large wind turbine blades”, and the financial support is greatly appreciated.

This work was funded by the VLAIO Innovation Mandate project number HBC.2016.0235.

References

[1] International Electrotechnical Commission. International standard iec 61400-23 Wind turbine generator systems – part 23: full-scale structural testing of rotor blades. Wind Turbines-Part 1: Design Requirements. (2014).

[2] GE Renewable Energy, GE announces Haliade-X, the world’s most powerful offshore wind turbine, (2018).

[3] P Avitabile, Modal testing : a practitioner's guide, John Wiley & Sons Ltd 2018.

[4] DJ Ewins, Modal testing: theory and practice, Research studies press Letchworth 1984.

[5] W Heylen, S Lammens, P Sas, Modal Analysis Theory and Testing, 2nd ed., Katholieke Universiteit Leuven, Departement Werktuigkunde, Leuven, 1998.

[6] GC Larsen, MH Hansen, A Baumgart, I Carlén, Modal analysis of wind turbine blades, Risø–R–1181(EN) (2002).

[7] HB Pedersen, OJD Kristensen. Applied modal analysis of wind turbine blades. (2003).

[8] DT Griffith, G Smith, M Casias, S Reese, TW Simmermacher. Modal Testing of the TX-100 Wind Turbine Blade, Sandia National Laboratories Technical Report, Report# SAND2005-6454. (2006).

[9] D Griffith, TG Carne. Experimental Uncertainty Quantification of Modal Test Data, Sandia National Laboratories (SNL-NM), Albuquerque, NM (United States). (No. SAND2006-6507C) (2006).

[10] MM Luczak, Uncertainty Quantification of the Main Rotor Blades Measurements, Recent Progress in Flow Control for Practical Flows, Springer, 2017, pp. 429-482.

[11] DT Griffith, TG Carne, Experimental modal analysis of 9-meter research-sized wind turbine blades, Structural Dynamics and Renewable Energy, Volume 1, Springer, 2011, pp. 1-14.

[12] US Paulsen, O Erne, M Klein, Modal analysis on a 500 kW wind turbine with stereo camera technique, International Operational Modal Analysis Conference. IOMAC. (2009).

[13] P Poozesh, J Baqersad, C Niezrecki, P Avitabile, E Harvey, R Yarala. Large-area photogrammetry based testing of wind turbine blades, Mechanical Systems and Signal Processing. 86 (2017) 98-115.

[14] P Poozesh, A Sarrafi, Z Mao, C Niezrecki. Modal parameter estimation from optically-measured data using a hybrid output-only system identification method, Measurement. 110 (2017) 134-145.

[15] FL dos Santos, B Peeters, Strain Modal Analysis, Recent Progress in Flow Control for Practical Flows, Springer, 2017, pp. 405-428.

[16] V Ruffini, T Nauman, C Schwingshackl, Impulse excitation of piezoelectric patch actuators for modal analysis, Topics in Modal Analysis & Testing, Volume 10, Springer, 2017, pp. 97-106.

[17] JR White, DE Adams, MA Rumsey, Modal analysis of CX-100 rotor blade and micon 65/13 wind turbine, Structural Dynamics and Renewable Energy, Volume 1, Springer, 2011, pp. 15-27.

[18] M Luczak, S Manzato, B Peeters, K Branner, P Berring, M Kahsin. Updating finite element model of a wind turbine blade section using experimental modal analysis results, Shock Vibrat. 2014 (2014).

[19] GC Larsen, P Berring, D Tcherniak, PH Nielsen, K Branner, Effect of a damage to modal parameters of a wind turbine blade, (2014).

[20] J Blasques, R Bitsche, V Fedorov, MA Eder, Applications of the beam cross section analysis software (becas), (2013) 46-49.

[21] J Schoukens, R Pintelon, Y Rolain, Mastering system identification in 100 exercises, John Wiley & Sons 2012.

[22] R Pintelon, J Schoukens, System identification: a frequency domain approach, John Wiley & Sons 2012.

[23] R Priemer, Introductory signal processing, World Scientific Publishing Company 1990.

[24] TP Dobrowiecki, J Schoukens. Linear approximation of weakly nonlinear MIMO systems, IEEE Transactions on Instrumentation and Measurement. 56 (2007) 887-894.

[25] P Guillaume, R Pintelon, J Schoukens. Accurate estimation of multivariable frequency response functions, IFAC Proceedings Volumes. 29 (1996) 4351-4356.

[26] P Csurcsia. Static nonlinearity handling using best linear approximation: An introduction, Pollack Periodica. 8 (2013) 153-165.